AIAA JOURNAL
Vol. 31, No. 11, November 1993

Three-Dimensional Simulations of Compressible Mixing Layers: Visualizations and Statistical Analysis

L. J. Leep,* J. C. Dutton,† and R. F. Burr‡
University of Illinois at Urbana-Champaign, Urbana, Illinois 61801

The effects of compressibility on the planar mixing layer are investigated by means of visualization and statistical analysis of the flowfield quantities computed using three-dimensional temporally evolving inviscid simulations. The levels of compressibility studied range from relative Mach numbers of $M_r = 0.2$–2.4. The objectives of this research are to identify large-scale structures present in the mixing layer at different levels of compressibility as well as to examine the statistical description of the flowfield, in order to gain understanding of the physical entrainment and mixing processes. Three-dimensional simulation visualizations of both the passive scalar and pressure fields show the nature of the large-scale structure present in the planar mixing layer to change from nearly two dimensional and spanwise at low compressibility to highly three dimensional and oblique at increased compressibility. Statistical analysis of the flowfield quantities shows that the shear layer width, Reynolds shear stress, and transverse turbulence intensity decrease with increasing compressibility levels, whereas the streamwise turbulence intensity remains nearly constant and the spanwise turbulence intensity increases. These statistics support the increasingly three-dimensional nature of the large-scale motion of the mixing layer with increasing M_r.

Nomenclature

a = sound speed
L_x = axial direction domain length or axial directional difference operator
L_y = transverse direction domain length or transverse directional difference operator
L_z = spanwise direction domain length or spanwise directional difference operator
M_c = convective Mach number $[\Delta U/(a_1+a_2)]$
M_r = relative Mach number $[2\Delta U/(a_1+a_2)]$
p = static pressure
$\boldsymbol{q}$ = conservation form solution vector
T = static temperature
U = axial direction mean velocity
ΔU = shear layer streamwise mean velocity difference
u = axial direction instantaneous velocity
v = transverse direction instantaneous velocity
w = spanwise direction instantaneous velocity
x = axial direction coordinate
y = transverse direction coordinate
z = spanwise direction coordinate or mixture fraction
α = axial wave number
β = spanwise wave number
θ = angle of instability wave
ρ = density
σ = turbulence intensity
$\langle\rangle$ = time or ensemble average

Introduction and Background

THE compressible free shear layer is a fundamental flow type that is currently of great research interest. These mixing layers are central to many advanced hypersonic propulsion system designs, such as the supersonic combustion ramjet engine. Many recent mixing layer studies examine compressibility effects as characterized by the relative Mach number M_r or convective Mach number M_c. The convective Mach number can be interpreted as the Mach number of the freestreams relative to a convective frame moving with the large-scale structures; the relative Mach number is based on the velocity difference across the mixing layer $M_r = \Delta U/\bar{a}$ and is twice the convective Mach number for freestreams having equal specific heat ratios. These Mach numbers have been shown to be effective for correlating trends observed in compressible mixing layers in comparison to incompressible mixing layers at the same freestream velocity and density ratios.[1–3]

Large-Structure Studies

Much research in recent years has focused on three-dimensional studies of compressible shear layers in order to understand the large-scale structure which governs this flow. This work has been in both the experimental and computational arenas. Investigations by Clemens,[4] Clemens and Mungal,[5] Messersmith,[6] and Messersmith et al.[7] used Mie scattering from condensed ethanol droplets to reveal large-scale structures in compressible shear layers at relative Mach numbers up to approximately 1.5. The large-scale spanwise structures are most clear and coherent in the lower compressibility flows, and plan views indicate that these structures are two dimensional in nature. As the compressibility of the mixing layer increases, plan views show an oblique orientation of the large-scale structures, followed by a complete breakdown into three dimensionality of the large-scale structures. Oblique or end views shown in the flow visualizations of Refs. 6 and 7 and in Refs. 4 and 5 show "jets" of unmixed fluid which seem to indicate the presence of counter-rotating vortices in the streamwise direction at moderate compressibility levels. Visualizations by Clemens[4] also show that the cross-sectional shape of the spanwise structures that are found in the compressible mixing layer are more polygonal and elongated in nature than those found at low relative Mach numbers which are nearly elliptic in shape. Rayleigh scattering results of Fourguette et al.[8] indicate an increased three dimensionality with increasing compressibility. Elliott et al.[9] also used Rayleigh scattering and showed the existence of large-scale structures with embedded smaller structure in a compressible mixing layer at $M_r = 1.72$. Further evidence of the existence of turbulent large-scale structure in compressible mixing layers was provided by Elliott et al.[10] who studied mixing layers at relative Mach numbers up to $M_r = 1.72$. They showed from pressure correlation mea-

Received June 26, 1992; Revision received March 1, 1993; accepted for publication March 10, 1993.

*Graduate Research Assistant, Department of Mechanical and Industrial Engineering; currently Research Engineer, Ford Research Labs, Suite 1100, 23400 Michigan Avenue, Dearborn, MI 48124. Member AIAA.

†Professor, Department of Mechanical and Industrial Engineering. Associate Fellow AIAA.

‡Graduate Research Assistant, Department of Mechanical and Industrial Engineering; currently Senior Scientist, Graphics Printing and Imaging Division, Tektronix, Inc., 26600 S.W. Parkway, Wilsonville, OR 97070.

surements that large two-dimensional spanwise-oriented structures dominate the mixing layer at low relative Mach numbers, tending to become oblique with increasing relative Mach number.

A host of shear layer numerical simulations have been performed recently, ranging from incompressible and two dimensional to compressible and three dimensional in nature. Several recent temporally and spatially evolving two-dimensional simulations of compressible mixing layers[11–15] were used to investigate inert shear layer stability and structure development. Large-scale structures evolve from the initial shear layer instabilities. These vortices continue to grow and eventually interact and pair. The spanwise vortices observed in these two-dimensional compressible mixing layer simulations tend to be somewhat rounded but are more flat and elongated than their incompressible counterparts. Growth rate reduction with increasing compressibility was also observed, which is in agreement with experimental findings. Three-dimensional compressible mixing layer simulations have recently been performed by Soetrisno et al.[15] and Sandham and Reynolds.[13,16,17] At low compressibility, the structures present in the mixing layer are similar to those found in incompressible cases: dominant two-dimensional spanwise vortices with embedded smaller scale streamwise counter-rotating vortices. These investigators, however, note that the three-dimensional oblique instability modes become increasingly important at higher relative Mach numbers ($M_r > 1.2$). The orientation of the most amplified oblique waves was found to follow the approximate relation $M_r \cos\theta \approx 1.2$, where θ is the angle between the wave and the spanwise direction. Sandham and Reynolds[13,17] identify three regimes that characterize compressible mixing layer stability as a result of their three-dimensional direct numerical simulations and stability analyses: 1) $0 < M_r < 1.2$, in which the two-dimensional spanwise instability is the most rapidly amplified; 2) $1.2 < M_r < 2.0$, in which the oblique wave is the most amplified wave, although the two-dimensional wave is still amplified and may have an effect; and 3) $M_r > 2.0$, in which the two-dimensional instability is considerably less amplified than the most unstable oblique wave. The three-dimensional nature of the compressible mixing layer was also suggested by the results of Soetrisno et al.,[15] Ragab and Sheen,[18] and Tuncer and Sankar,[19] who have shown that the perturbation energy associated with two-dimensional disturbances grows much slower than that associated with three-dimensional disturbances in mixing layers with a relative Mach number greater than 1.2.

Turbulence Statistics Studies

Many previous experimental studies of planar mixing layers have involved the measurement of various turbulence quantities within the fully developed region of the flow. Although several investigators have published data concerning incompressible mixing layer turbulence statistics, such information for compressible mixing layers is much more limited. An extensive review of the literature concerning the turbulence statistics of planar, two-dimensional, incompressible mixing layers has recently been compiled by Gruber.[20] The two-dimensional measurements of Elliott and Samimy[3] and Samimy and Elliott[21] show decreasing peak streamwise and transverse turbulence intensities and peak normalized Reynolds shear stress with increasing relative Mach number. At the highest compressibility level investigated, the streamwise and transverse peak turbulence intensities were reduced by 30 and 35%, respectively, as compared to incompressible results.[22–24] The normal stress anisotropy (σ_u/σ_v), however, remained roughly constant since the peak streamwise and transverse turbulence intensities decreased at approximately the same rate with increasing compressibility. Two-component laser Doppler velocimetry (LDV) data gathered by Goebel and Dutton[1] and Goebel[25] show that the peak transverse turbulence intensity and normalized Reynolds shear stress decrease with increasing compressibility in agreement with Elliott and Samimy.[3] However, the streamwise turbulence intensity was shown to remain relatively constant with increasing relative Mach number. At the highest relative Mach number studied, the peak transverse turbulence intensity and normalized Reynolds shear stress are reduced by 45 and 40%, respectively, over the incompressible values although the streamwise turbulence intensity shows no reduction. Thus, there is a substantial increase in normal stress anisotropy with increasing compressibility. Three-dimensional statistical data for a compressible mixing layer at $M_r = 1.59$ have recently been published by Gruber.[20] This study found that the peak streamwise and spanwise turbulence intensities remain nearly constant as compared to the incompressible values, whereas the peak transverse turbulence intensity and the peak normalized Reynolds shear stress decrease with increasing relative Mach number.

Most shear layer numerical simulations have focused on visualizations or stability analyses. Very few investigators have exploited the capability of the simulations to calculate the turbulence statistics from the flow quantities computed. An exception is the two-dimensional incompressible inviscid simulations of Chien et al.[26] who computed statistics associated with large-scale motion. In these simulations, the peak transverse turbulence intensity was found to be slightly greater than or nearly equal to the streamwise turbulence intensity for the incompressible cases studied. Two-dimensional compressible simulations performed by Burr[14] and Burr and Dutton[27] attempted to capture the energy-containing activity of the compressible shear layer. The statistical data computed from the simulations show that the normal stress anisotropy ratio σ_u/σ_v increases from approximately 1.5 for the incompressible case to approximately 3.5 for the compressible case. The primary normalized Reynolds shear stress and the shear layer growth rate were shown to decrease with increasing compressibility.

Objectives

In an area where a plethora of research, both experimental and numerical, has been performed, many aspects of this seemingly simple shear flow still are unexplained and unexplored. The inviscid simulations presented here can be used to examine the physical entrainment and mixing processes of compressible shear layers by observing the large-scale structures and studying the statistics related to large-scale motion. These simulations examine the effects of compressibility levels higher than those previously studied experimentally or numerically. An additional advantage of these simulation visualizations is the ability to examine, at relatively low cost, a nearly infinite number of views of the flowfield. Pressure, vorticity, and scalar fields can be visualized to aid in the understanding of the physical nature of this flow. The specific objectives of the work presented herein are to 1) develop and validate a three-dimensional mixing layer simulation code using a time-split symmetric explicit predictor-corrector total variational diminishing (TVD) scheme, 2) compare the simulation results with recent experimental and computational results, 3) use the many views available from the simulation results to determine and explain the effects of compressibility on the large-scale structure of turbulent mixing layers, and 4) determine the effects of compressibility on the statistical quantities describing the behavior of a planar shear layer.

Mathematical Model and Numerical Methodology

For the simulations presented herein, the governing equations are the time-dependent Euler equations and, for these nonreacting simulations, the transport of a passive scalar (mixture fraction) is also considered. Although viscous diffusion can be included, it does not affect the basic inviscid instabilities responsible for the larger scale motions that dominate the transport processes in compressible mixing layers. Therefore, only implicit numerical diffusion is included in the simulations presented here.

A schematic of the temporally evolving mixing layer geometry is shown in Fig. 1. Temporally evolving shear layers are often studied as a computationally more efficient alternative to spatially evolving shear layers. Sigalla et al.[28] discuss the correlation between temporal and spatial results for compressible shear layer analysis. For the current three-dimensional simulations, a time-split symmetric explicit predictor-corrector TVD code has been developed. The time-step split scheme involves the sequential application of the three directional difference operators (L_x, L_y, L_z)

$$\boldsymbol{q}^{n+2} = L_x, L_y, L_z, L_z, L_y, L_x \boldsymbol{q}^n \tag{1}$$

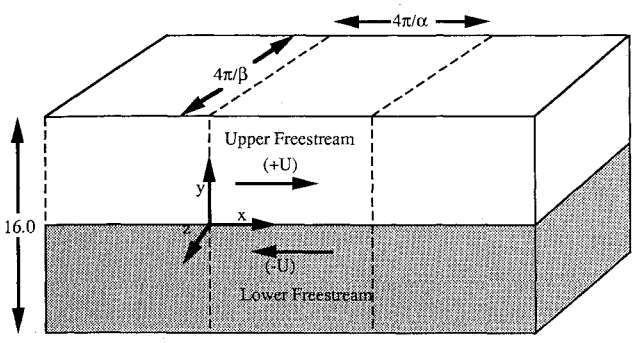

Fig. 1 Temporal shear layer schematic.

To ensure second-order time accuracy, the order of steps is symmetric. The equations are differenced in conservation form; to avoid bias due to one-sided differencing, the direction of differencing is alternated. Thus, in a two-step cycle, the order of operator application is reversed as well as the direction of differencing. Each directional difference operator (L_x, L_y, L_z) involves a series of three steps: a predictor step p, a corrector step c, and a TVD step t. The details of this numerical scheme can be found in Ref. 29.

Initial and Boundary Conditions

The temporally evolving shear layer simulations are initialized with a hyperbolic tangent mean streamwise velocity profile and zero mean transverse and spanwise velocities. All of the thermodynamic properties (pressure, temperature, and density) are initialized to uniform values. The mixture fraction is initialized with a narrow hyperbolic tangent profile. Inlet and outlet as well as front and back (z direction in Fig. 1) boundary conditions are treated as periodic. Upper and lower (y direction) boundaries are treated as free-slip walls and ensure that the mixing layer remains centered throughout the calculation.

The three velocity components, temperature, pressure, and density, are perturbed with small amplitude perturbations that correspond to the most unstable waves from linear stability analysis, as discussed in Ref. 29. The perturbation to each mean flow quantity profile consists of four waves: a two-dimensional spanwise fundamental wave, a two-dimensional spanwise subharmonic wave, and two equal and oppositely opposed oblique waves. The fundamental two-dimensional wave in this perturbation produces the instability which forms the spanwise rollers. The pairing of these vortices is induced by the subharmonic perturbation, which has a period twice that of the fundamental perturbation. The phase angle between the fundamental and subharmonic modes is selected to be $\pi/2$ to enhance pairing. The two equal and oppositely opposed oblique waves perturb three-dimensional motion in the mixing layer, thereby promoting the formation of counter-rotating streamwise vortices.

For the low-compressibility cases discussed subsequently ($M_r = 0.2$, $M_r = 0.8$), the two-dimensional wave is the most amplified wave. Thus, the x-direction wave number α that provides maximum amplification of this fundamental wave determines the initial conditions for this case. The oblique waves, although not as strongly amplified at these Mach numbers as the two-dimensional fundamental wave, are important since they perturb three-dimensional motion. For the more compressible cases ($M_r = 1.6$, $M_r = 2.4$), the oblique waves are the most amplified waves. Thus, the x- and z-direction wave numbers (α and β) that provide maximum amplification of the oblique waves determine the initial conditions for these cases. As previously mentioned, the orientation of the oblique disturbances follows the approximate form $M_r \cos\theta \approx 1.2$. Although not dominant, the two-dimensional spanwise waves are not negligible for these cases, since these waves are still necessary to stimulate formation of the large two-dimensional structures.

Code Validation and Grid Independence

To validate the three-dimensional aspects of the code, shock tube test cases were run in the three coordinate directions. In the test case shock tube flow, a right-running normal shock wave and an oppositely directed expansion fan are created due to the initial pressure difference across a diaphragm. In addition, a contact discontinuity moves to the right at a lower velocity than the shock wave. The computed results of the shock tube experiment are identical in all three coordinate directions and compare well with the analytical solution. Further information regarding this validation case can be found in Ref. 29.

All of the compressible mixing layer simulations were performed using a $97 \times 97 \times 97$ Cartesian grid on a Cray Y-MP supercomputer. The simulation code used to produce the results presented herein runs at approximately 120 mflops. The CPU time required to compute each simulation ranges from 2 to 4 h, with an average computation rate of 400 time steps per hour. To show that these calculations are grid independent, the $M_r = 0.8$ simulation was performed on a reduced $65 \times 65 \times 65$ Cartesian grid, and select averaged turbulence statistics were computed. The statistics determined using the results from the $65 \times 65 \times 65$ grid were very similar to those from the $97 \times 97 \times 97$ grid used for the bulk of the simulations. Thus, from the statistical data computed for the two simulations run on different grids, it can be safely assumed that the flowfields determined by these simulations are grid independent.

Results

The temporally evolving shear layer simulation code just described has been used to examine the effects of compressibility on the basic shear layer structure and statistical description. The current inviscid simulations attempt to resolve only the large scales or energy-containing motion, which tend to dominate the physics of this turbulent compressible shear flow. Thus, information on dissipation scale processes cannot be determined from the simulation results. Nevertheless, this type of simulation is still of substantial value for gaining insight into the physics and structure of turbulent compressible mixing layers.

The four cases considered in this study are described in Table 1. Case 1 is an incompressible case with a relative Mach number of $M_r = 0.2$, and case 2 is a low-compressibility case with a relative Mach number of $M_r = 0.8$. Cases 3 and 4 are compressible cases having relative Mach numbers of $M_r = 1.6$ and 2.4, respectively. These cases were selected to study the three regimes of stability suggested by Sandham and Reynolds[13,16,17] discussed earlier. It should be noted that since the simulations are inviscid, the values of the dimensional parameters in Table 1 are arbitrary.

The computational domain is shown in Fig. 1. The y-direction domain length L_y remains constant for all four simulation cases at a value of 16.0. The x- and z-direction domain lengths change for each case depending on the x- and z-direction wave numbers (α and β) computed from stability analysis. These domain lengths are of the form $L_x = 4\pi/\alpha$ and $L_z = 4\pi/\beta$, respectively.

Visualizations of the temporally evolving shear layer simulations are presented using gray scale maps of mixture fraction z and pressure p to qualitatively understand the structure and physics of the shear layer entrainment and mixing processes. The three-dimensional mixture fraction and pressure surface plots have the same orientation as the computational domain shown in Fig. 1. The statistical parameters are obtained by Favre averaging over an x-z plane for multiple time frames. The time frames used for the analysis of each case are evenly spaced in time and cover the same portion of the shear layer evolution process. The statistical analysis was performed between times when the shear layer has developed into two distinct spanwise rollers and just before the two rollers pair.

Table 1 Temporally evolving shear layer simulation conditions

Case	(1)	(2)	(3)	(4)
M_r	0.2	0.8	1.6	2.4
ΔU, m/s	126	126	126	126
ρ_i, kg/m3	0.35	0.35	0.35	0.35
T_i, K	1000	61.7	15.7	6.89
p_i, kPa	100	6.17	1.57	0.689
a_i, m/s	634	158	79	52.5

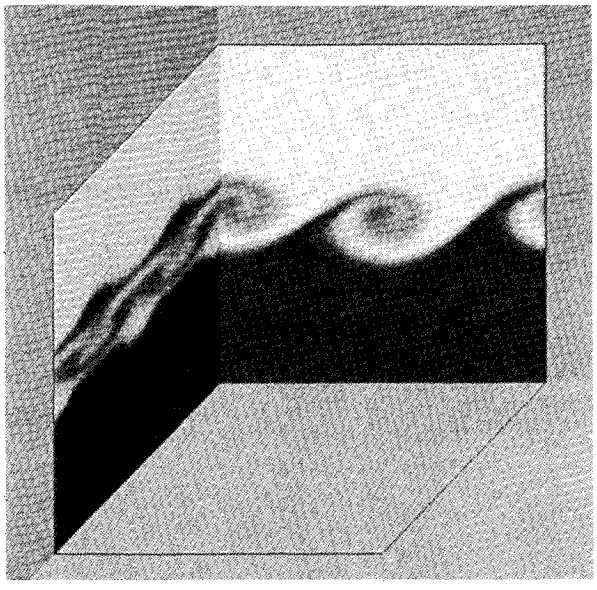

Fig. 2 Views of the mixture fraction field for the $M_r = 0.8$ mixing layer at time plane number 300.

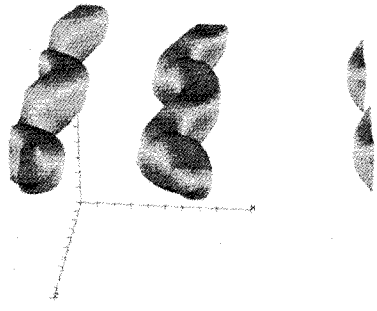

Fig. 3 Constant pressure surface plot for the $M_r = 0.8$ mixing layer at time plane number 390.

Visualizations

The visualizations of the incompressible $M_r = 0.2$ case are not shown here because they closely resemble those of the $M_r = 0.8$ case. The low-compressibility case, $M_r = 0.8$, is in the regime dominated by two-dimensional spanwise-oriented structures. The length of the domain for the $M_r = 0.8$ simulation in the streamwise and spanwise directions is $L_x = L_z = 15.40$, and the length in the transverse direction is $L_y = 16.0$. Figure 2 shows mixture fraction plots for the $M_r = 0.8$ case. The rollups seen in the side view of Fig. 2 are very similar to those computed in two-dimensional low compressibility simulations by Burr,[14] Burr and Dutton,[27] McMurtry et al.,[30] and Sandham and Reynolds.[13,16] They show the rounded Brown-Roshko[31] spanwise structures visualized by many experimentalists in incompressible shear layers. As the simulations progress in time, the two spanwise vortices interact and pair, forming a single structure. Streamwise structures are also apparent at this point in the temporal evolution; these mushroom-type structures form in the strained interfaces between the rollers. This type of structure has been seen in several experimental studies of incompressible mixing layers; the most notable visualizations which show this mushroom shape are the laser-induced fluorescence (LIF) visualizations of Bernal and Roshko.[32]

Visualizations of the pressure field have proven to be extremely helpful in understanding the fundamental structure of the mixing layer. Low-pressure regions are associated with strong rotation (i.e., vortex cores) which, in turn, identify the areas where the most mixing occurs. A perspective view of a constant pressure surface for the $M_r = 0.8$ case at a point in the evolution process where the two original spanwise vortices have developed but have not yet paired is shown in Fig. 3. This time plane is captured slightly after the time plane used to show the mixture fraction field in Fig. 2. The predominantly two-dimensional spanwise nature of the rollers, which have periodic bends in the spanwise direction, is quite clear. The pressure of the surface plotted is approximately 25% above the pressure minimum. This surface plot is similar to that shown by Sandham and Reynolds[13,17] for a low-compressibility mixing layer.

The moderate-compressibility case, $M_r = 1.6$, is in the regime where the three-dimensional oblique disturbances are more amplified than the two-dimensional spanwise disturbance, but amplification of both types of disturbances is significant. Thus, at this relative Mach number the structures that develop are expected to show increasing three dimensionality but also show large-scale spanwise vortices. The length of the domain for the $M_r = 1.6$ simulation in the streamwise and spanwise directions is $L_x = L_z = 24.21$, and the length in the transverse direction is $L_y = 16.0$. Figure 4 shows one of the two large-scale spanwise structures in the side view and two pairs of counter-rotating streamwise-oriented vortices in the end view. The large-scale spanwise structures shown in the side view of Fig. 4 appear more polygonal in shape than the corresponding low-compressibility structures, which are very elliptical or rounded. This observation is in agreement with the experimental visualizations of Clemens[4] who found polygonal structures at a relative Mach number of 1.58. The counter-rotating streamwise vortices visible in the end view of Fig. 4 are present in the braid region between the spanwise structures and wrap around neighboring vortices. These structures are very similar to those seen by Messersmith[6] in the oblique views of his Mie scattering

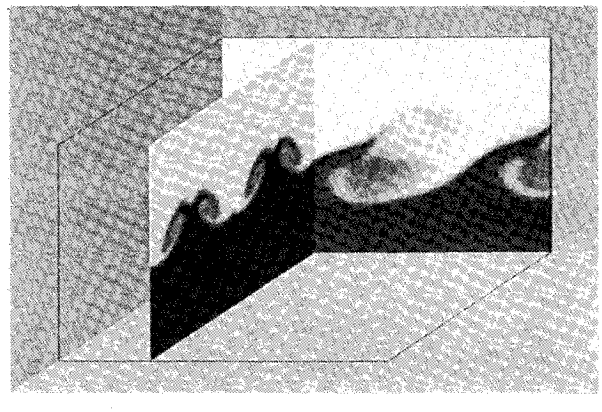

Fig. 4 Views of the mixture fraction field for the $M_r = 1.6$ mixing layer at time plane number 300.

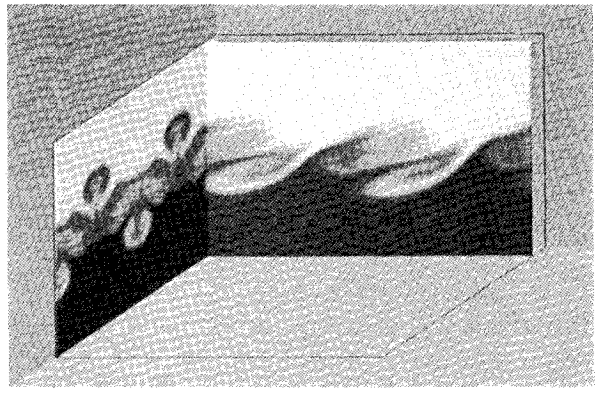

Fig. 5 Views of the mixture fraction field for the $M_r = 1.6$ mixing layer at time plane number 300.

shear layer visualizations. The end view in Fig. 5 shows four pairs of streamwise counter-rotating vortices. The four sets of counter-rotating vortices consist of two sets of small vortices situated in the top and bottom streams. The small streamwise vortices that are seen in the top stream are those that have ridden up the back of the spanwise structure and are near the top of the structure. The other sets of streamwise counter-rotating vortices, which are in the lower stream, are much farther apart (the two vortices that appear together are actually from two different pairs) than those in the top stream and are vortices that start in the braid region near the saddle point. The spacing of the streamwise vortices which constitute a pair shows that the structures are oriented at an oblique angle to the streamwise direction and ride up the back of the spanwise structures. The larger structures seen in the middle of the shear layer in the end view of Fig. 5, which appear to be streamwise counter-rotating vortices, are formed by three-dimensional mixing which occurs in the vortex cores but are not the counter-rotating vortices that form ribs on the large-scale spanwise rollers. An interesting phenomenon is captured by the side view scalar plot shown in Fig. 5. At approximately $z = L_z/8$, the spanwise large-scale structures appear to be composed of two smaller substructures. This was not seen in the lower compressibility case. This smaller scale composition could account for the more jagged nature of the large-scale structures noted at higher relative Mach number as observed by Messersmith[6] in his Mie scattering visualizations.

The nature of the low-pressure surfaces is again useful in understanding the underlying structure for this compressibility condition. The pressure plot presented in Fig. 6 shows a surface at approximately 30% above the pressure minimum for the case of $M_r = 1.6$. This time plane is taken at 150 steps after that shown in Figs. 4 and 5. This pressure plot shows an increasingly three-dimensional structure compared to the predominantly two-dimensional spanwise-oriented pressure surface plot shown in Fig. 3 for $M_r = 0.8$. The oblique structures in Fig. 6 show a preferential orientation of approximately ± 45 deg to the spanwise direction, which is in agreement with stability theory. There is also seen in this plot some reminiscence of the two-dimensional bent tubes seen in the low-compressibility visualizations. The shape of these pressure surfaces agrees well with those computed from the results

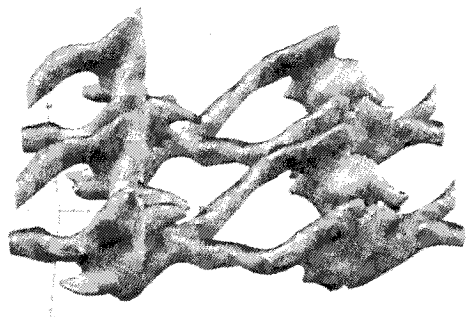

Fig. 6 Constant pressure surface plot for the $M_r = 1.6$ mixing layer at time plane number 450.

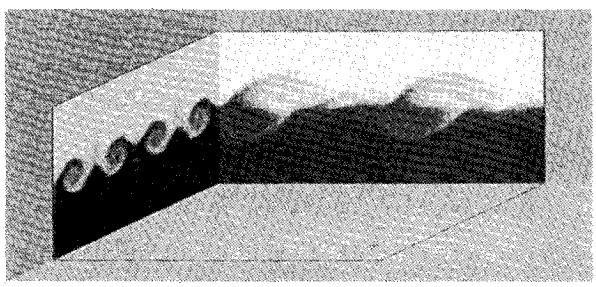

Fig. 7 Views of the mixture fraction field for the $M_r = 2.4$ mixing layer at time plane number 300.

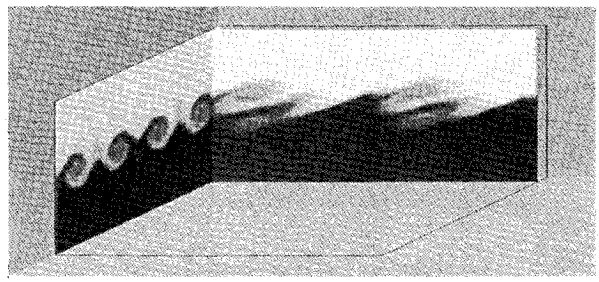

Fig. 8 Views of the mixture fraction field for the $M_r = 2.4$ mixing layer at time plane number 300.

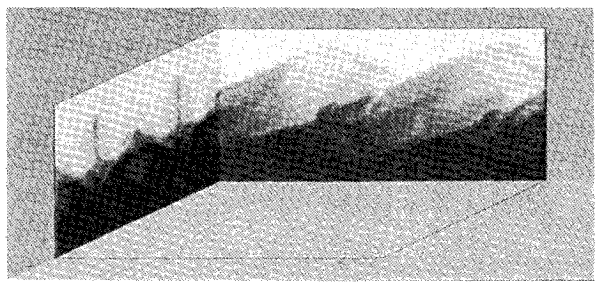

Fig. 9 Views of the mixture fraction field for the $M_r = 2.4$ mixing layer at time plane number 450.

of three-dimensional direct numerical simulations performed by Sandham and Reynolds[13] for a similar case.

The visualizations of the highest compressibility case considered here ($M_r = 2.4$) show several interesting results. This $M_r = 2.4$ case is in the regime where oblique disturbances are the only disturbances which are significantly amplified. Thus, the structures which develop are expected to be highly three dimensional. This does not necessarily imply that large-scale structures will not be present, but instead that these large-scale structures will not appear as two-dimensional spanwise-oriented rollers as seen at lower compressibility. The lengths of the domain for the $M_r = 2.4$ simulation in the streamwise and spanwise directions are $L_x = 34.15$ and $L_z = 19.72$, and the length in the transverse direction is $L_y = 16.0$. Figure 7 shows somewhat spiked spanwise structures in the side view and two pairs of distinct counter-rotating streamwise vortices in the end view. A move forward in the z-direction by approximately $L_z/16$ shows two smaller spanwise substructures which appear to form one larger and seemingly more squared off structure (Fig. 8).

The visualization in Fig. 9 shows the structure in the $M_r = 2.4$ shear layer after it has developed further temporally than that seen in Figs. 7 and 8. The large-scale spanwise structures now appear quite jagged. Thus, the changes in the spanwise structure proceed from elliptical rollers at low-compressibility conditions ($M_r = 0.8$) to squared off and somewhat jagged structures at moderate compressibility ($M_r = 1.6$) to very angular and jagged structures at high compressibility ($M_r = 2.4$). The end view in Fig. 9 also shows thin but long transverse spikes in place of the counter-rotating vortices present in the earlier time frame (Fig. 7). As discussed earlier, similar transverse "jets" have been visualized experimentally by Clemens[4] and Messersmith.[6]

The constant pressure surface plot in Fig. 10 reinforces the dominance of the oblique structure at $M_r = 2.4$. The surface plotted in Fig. 10 is approximately 25% above the pressure minimum at this time plane. This is approximately the same time plane used to show the mixture fraction field in Figs. 7 and 8. There are no hints of two-dimensional spanwise structure in this figure, but rather the oblique tubes which form V-structures are clearly the dominant structures. This pressure surface plot is similar to that shown by Sandham and Reynolds[13] for simulations at $M_r = 2.1$, although the V structures are more pronounced in the pressure plot in Fig. 10 than in those by Sandham and Reynolds.[13] This is most likely due to the higher level of compressibility in the present simulations.

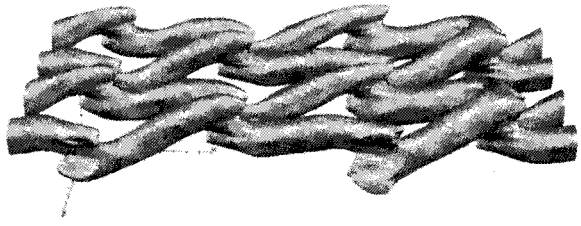

Fig. 10 Constant pressure surface plot for the $M_r = 2.4$ mixing layer at time plane number 290.

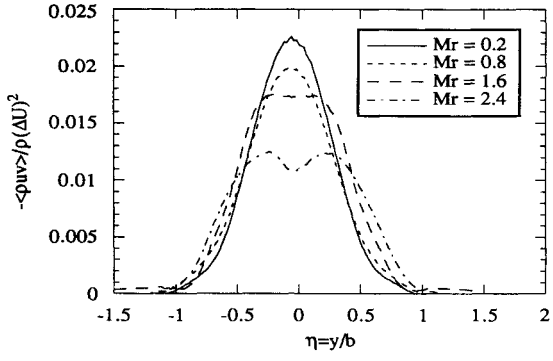

Fig. 11 Reynolds shear stress profile comparison.

Statistical Analysis

The mean axial velocity profiles for the four cases studied, which were computed but are not shown here, are similar in shape to the profiles of experimental data and show that the effect of compressibility on the mean velocity profile shape is negligible.[25] The shear layer width, which is considered here to be the distance between the transverse locations at which $U = U_1 - 0.1\Delta U$ and $U = U_2 + 0.1\Delta U$, where U_1 and U_2 are the two freestream velocities, was shown to grow more slowly in time (and thus in space for the spatially evolving case) as compressibility is increased. This reduction in growth rate is directly related to the decrease in normalized Reynolds shear stress with increasing compressibility. Figure 11 shows the normalized Reynolds shear stress profiles, $-\langle\rho uv\rangle/\rho(\Delta U)^2$, for the four cases considered. The reduction of mixing layer width and reduction in Reynolds shear stress (Fig. 11) with increasing compressibility are in agreement with recent experimental data[1,3,20] and with the results of the two-dimensional simulations of Burr and Dutton.[27] In experimental results, the peak magnitude as well as the lateral extent of the shear stress profile both decrease with increasing compressibility. The two other normalized Reynolds shear stresses, $-\langle\rho uw\rangle/\rho(\Delta U)^2$ and $-\langle\rho vw\rangle/\rho(\Delta U)^2$, were also computed. As expected, they were both nearly identically zero at all of the locations in the shear layer and at all levels of compressibility and, therefore, are not shown graphically.

Figures 12–15 show turbulence intensity (Reynolds normal stress) profiles, $\sigma_u/\Delta U$, $\sigma_v/\Delta U$, and $\sigma_w/\Delta U$, for the various cases considered. By comparing the four plots, the normal stress anisotropy ratio σ_u/σ_v can be seen to increase from approximately unity (based on peak values of σ_u and σ_v) for the lowest compressibility case to nearly 1.6 for the highest compressibility case. Although somewhat smaller in magnitude, this increase in the σ_u/σ_v anisotropy with increasing compressibility is qualitatively in agreement with the trend of the experimental data of Goebel and Dutton.[1] On the other hand, the experiments of Elliott and Samimy[3] show a nearly constant σ_u/σ_v anisotropy ratio. Also, in agreement with the experimental data of Goebel and Dutton,[1] the increase in anisotropy with increasing compressibility is due primarily to the decrease in transverse turbulence intensity $\sigma_v/\Delta U$. The magnitude of the streamwise turbulence intensity is shown to be nearly independent of compressibility level at a value of approximately $\sigma_u/\Delta U = 0.20$. This value is only slightly higher than the experimentally observed constant streamwise turbulence intensity of Goebel and Dutton[1] which is approximately 0.18. This is in excellent agreement with the experiments since the small dissipation scale motion is not considered in these simulations; thus, the value computed from the present simulations is expected to be greater than that for a real flow.

The growth of the spanwise turbulence intensity $\sigma_w/\Delta U$ with increasing compressibility is also illustrated in Figs. 12–15. The anisotropy ratio σ_u/σ_w decreases substantially with increasing relative Mach number from approximately 1.6 to just below 1.0 primarily due to the increase in $\sigma_w/\Delta U$ with increasing compressibility. This growth in the spanwise component with increasing compressibility agrees with visualizations that show the nature of the large-scale structures in the shear layer to become more three dimensional. The energy in the transverse component is redistributed to the spanwise component via pressure strain.[29] This result, however, disagrees with the experimental data of Gruber[20] who found the anisotropy ratio of σ_u/σ_w to remain nearly constant over a range of compressibilities up to $M_r = 1.6$. Except for the small central peak in the spanwise turbulence intensity profile, the simulation results in Fig. 14 for $M_r = 1.6$ agree extremely well qualitatively with the trends of Gruber's[20] data, showing $\sigma_u/\Delta U$ having the largest magnitude and $\sigma_v/\Delta U$ the smallest magnitude with $\sigma_w/\Delta U$ having an intermediate value. The relatively low values of $\sigma_w/\Delta U$ in the two low-compressibility simulations ($M_r = 0.2$ and $M_r = 0.8$) may be due to the lack of development of the three-dimensional structures at the point in the evolution process when the statistics are computed (i.e., using several time planes spanning the time between development of the two spanwise rollers to a point just before pairing). Thus, the spanwise direction statistics may not accurately represent an actual spatially evolving shear layer for the two low-compressibility cases. The trends, however, provide useful information. The nearly constant peak spanwise turbulence intensity for the two more compressible cases ($M_r = 1.6$ and 2.4) may indeed be correct since the three-dimensional structures develop

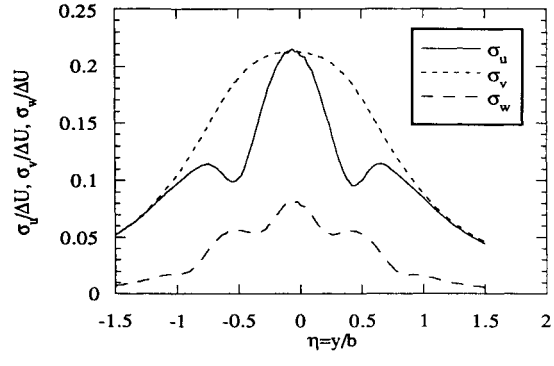

Fig. 12 $M_r = 0.2$ turbulence intensities.

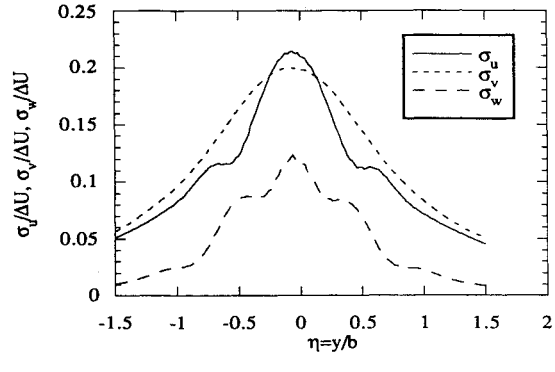

Fig. 13 $M_r = 0.8$ turbulence intensities.

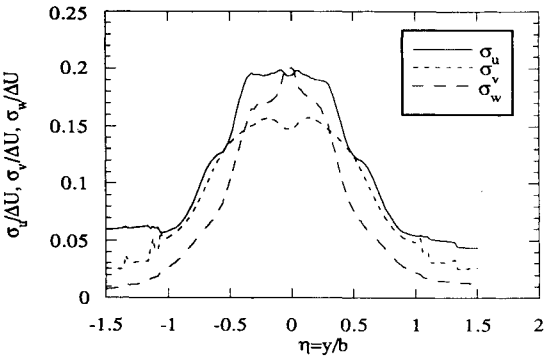

Fig. 14 $M_r = 1.6$ turbulence intensities.

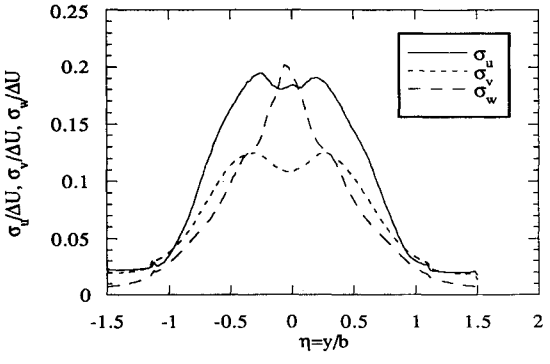

Fig. 15 $M_r = 2.4$ turbulence intensities.

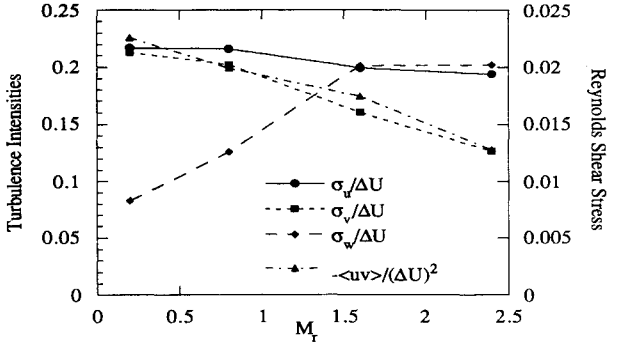

Fig. 16 Peak turbulence intensities and Reynolds shear stresses.

early in the simulations for these cases. Thus, it can be theorized from both the experimental and simulation results available that the spanwise turbulence intensity may increase only slightly with increased levels of compressibility. At this time, however, no experimental data are available with which to compare the computed results for the $M_r = 2.4$ case.

A summary of the turbulence intensity dependence on relative Mach number, as well as the Reynolds shear stress results, is presented in Fig. 16. The relatively constant streamwise turbulence intensity is shown in contrast to the decreasing and increasing transverse and spanwise turbulence intensities, respectively. These statistical results for the turbulence intensities are clearly in good agreement with the visualizations presented earlier that show a shift from rounded, spanwise-oriented structures at low-compressibility to more angular, flattened, and obliquely oriented structures at higher compressibility. The normalized Reynolds shear stress decreases in the same manner as the transverse turbulence intensity as relative Mach number increases. This trend is identical to the one found experimentally by Goebel and Dutton.[1] These results demonstrate that a primary effect of compressibility is to suppress the transverse velocity fluctuations.

Reference 29 discusses several additional statistical quantities for which space is not available in the present paper. These include the velocity correlation coefficient, passive scalar mean and standard deviation, normal stress production, and pressure-dilatation and pressure-strain terms.

Conclusions

The explicit three-dimensional time-split predictor-corrector TVD code developed herein was found to accurately and robustly simulate inert shear layers over a range of compressibility levels. Visualizations of a passive scalar for two of the cases ($M_r = 0.8$ and 1.6) have been compared to and found to agree with several observations from previous experimental results and with other numerical simulations. Pressure field visualizations at the various compressibility levels considered also concur with those obtained from numerical simulations performed by other researchers. The flowfield quantities computed from three-dimensional temporally evolving numerical simulations have been statistically analyzed to further investigate the effects of compressibility on mixing layer behavior. The $M_r = 2.4$ case represents an extension to a higher compressibility level than examined in previous numerical or experimental work.

Several of the more important conclusions that may be drawn from the results of the present compressible mixing layer visualization and statistical studies are as follows:

1) The cross-sectional shape of the large-scale, spanwise structures changes with increasing compressibility; the structures are rounded and elliptical at low-compressibility conditions, becoming increasingly polygonal and angular in shape at increased levels of compressibility.

2) The spanwise large-scale structures present in the moderate- to high-compressibility cases appear to be composed of two smaller substructures that cause the jagged nature observed experimentally.

3) Constant pressure surface plots reveal the underlying structure of the compressible shear layer to be highly two dimensional and spanwise oriented at low compressibility and increasingly three dimensional and obliquely oriented at higher compressibility.

4) The normalized Reynolds shear stress and the normalized mixing layer growth rate decrease with increasing compressibility.

5) The peak streamwise turbulence intensity $\sigma_u/\Delta U$ remains at a relatively constant value over a wide range of compressibility.

6) The peak transverse turbulence intensity $\sigma_v/\Delta U$ decreases with increasing compressibility causing the normal stress anisotropy ratio σ_u/σ_v to increase with compressibility.

7) The peak spanwise turbulence intensity $\sigma_w/\Delta U$ increases (perhaps only modestly) with compressibility causing the anisotropy ratio σ_u/σ_w to decrease with increasing compressibility.

8) A primary effect of compressibility on the shear layer is to suppress transverse velocity fluctuations which is implied by the reduction in both the normalized Reynolds shear stress and the peak transverse turbulence intensity.

Acknowledgments

The authors would like to acknowledge the financial support provided by the Air Force Wright Laboratories with A. S. Nejad as Contract Monitor, and the computer resources provided by the National Science Foundation National Center for Supercomputing Applications. Thanks also go to Olivier Planche at Stanford University for his assistance with the stability analysis portion of this work.

References

[1]Goebel, S. G., and Dutton, J. C., "Experimental Study of Compressible Turbulent Mixing Layers," *AIAA Journal*, Vol. 29, No. 4, 1991, pp. 538–546.

[2]Papamoschou, D., and Roshko, A., "The Compressible Turbulent Shear Layer: An Experimental Study," *Journal of Fluid Mechanics*, Vol. 197, Dec. 1988, pp. 453–477.

[3]Elliott, G. S., and Samimy, M., "Compressibility Effects in Free Shear

Layers," *Physics of Fluids A*, Vol. 2, No. 7, 1990, pp. 1231–1240.

[4]Clemens, N. T., "An Experimental Investigation of Scalar Mixing in Supersonic Turbulent Shear Layers," Dept. of Mechanical Engineering, Stanford Univ., Rept. T-274, Stanford, CA, 1991.

[5]Clemens, N. T., and Mungal, M. G., "Two- and Three-Dimensional Effects in the Supersonic Mixing Layer," *AIAA Journal*, Vol. 30, No. 4, 1992, pp. 973–981.

[6]Messersmith, N. L., "An Experimental Investigation of Organized Structure and Mixing in Compressible Turbulent Free Shear Layers," Ph.D. Thesis, Dept. of Mechanical and Industrial Engineering, Univ. of Illinois at Urbana-Champaign, Urbana, IL, Jan. 1992.

[7]Messersmith, N. L., Dutton, J. C., and Krier, H., "Experimental Investigation of Large Scale Structures in Compressible Mixing Layers," AIAA Paper 91-0244, Jan. 1991.

[8]Fourguette, D. C., Mungal, M. G., Barlow, R. S., and Dibble, R. W., "Concentration Measurements in a Supersonic Shear Layer," AIAA Paper 91-0627, Jan. 1991.

[9]Elliott, G. S., Samimy, M., and Arnette, S. A., "A Study of Compressible Mixing Layers Using Filtered Rayleigh Scattering," AIAA Paper 92-0175, Jan. 1992.

[10]Elliott, G. S., Samimy, M., and Reeder, M. F., "Pressure-Based Real-Time Measurements in Compressible Free Shear Layers," AIAA Paper 90-1980, July 1990.

[11]Soetrisno, M., Eberhardt, S., Riley, J. J., and McMurtry, P., "A Study of Inviscid, Supersonic Mixing Layers Using a Second-Order TVD Scheme," AIAA Paper 88-3676, June 1988.

[12]Greenough, J., Riley, J. J., Soetrisno, M., and Eberhardt, D., "Effects of Walls on a Compressible Mixing Layer," AIAA Paper 89-0372, Jan. 1989.

[13]Sandham, N. D., and Reynolds, W. C., "A Numerical Investigation of the Compressible Mixing Layer," Dept. of Mechanical Engineering, Stanford Univ., Rept. TF-45, Stanford, CA, Sept. 1989.

[14]Burr, R. F., "Numerical Modeling and Simulation of Compressible Reacting Turbulent Shear Layers," Ph.D. Thesis, Dept. of Mechanical and Industrial Engineering, Univ. of Illinois at Urbana-Champaign, Urbana, IL, May 1991.

[15]Soetrisno, M., Greenough, J. A., Eberhardt, D. S., and Riley, J. J., "Confined Compressible Mixing Layers: Part I. Three-Dimensional Instabilities," AIAA Paper 89-1810, June 1989.

[16]Sandham, N. D., and Reynolds, W. C., "Compressible Mixing Layer: Linear Theory and Direct Simulation," *AIAA Journal*, Vol. 28, No. 4, 1990, pp. 618–624.

[17]Sandham, N. D., and Reynolds, W. C., "Three-Dimensional Simulations of Large Eddies in the Compressible Mixing Layer," *Journal of Fluid Mechanics*, Vol. 224, 1991, pp. 133–158.

[18]Ragab, S. A., and Sheen, S., "Large-Eddy Simulation of a Mixing Layer," AIAA Paper 91-0233, Jan. 1991.

[19]Tuncer, I. H., and Sankar, L. N., "Numerical Simulation of Three-Dimensional Supersonic Free Shear Layers," *AIAA Journal*, Vol. 30, No. 4, 1992, pp. 871, 872.

[20]Gruber, M. R., "Three-Dimensional Velocity Measurements in a Turbulent, Compressible Mixing Layer," M.S. Thesis, Dept. of Aeronautical and Astronautical Engineering, Univ. of Illinois at Urbana-Champaign, Urbana, IL, Jan. 1992.

[21]Samimy, M., and Elliott, G. S., "Effects of Compressibility on the Characteristics of Free Shear Layers," *AIAA Journal*, Vol. 28, No. 3, 1990, pp. 439–445.

[22]Oster, D., and Wygnanski, I., "The Forced Mixing Layer Between Parallel Streams," *Journal of Fluid Mechanics*, Vol. 123, Oct. 1982, pp. 91–130.

[23]Mehta, R. D., and Westphal, R. V., "Near-Field Turbulence Properties of Single- and Two-Stream Plane Mixing Layers," *Experiments in Fluids*, Vol. 4, No. 5, 1986, pp. 257–266.

[24]Bell, J. H., and Mehta, R. D., "Development of a Two-Stream Mixing Layer from Tripped and Untripped Boundary Layers," AIAA Paper 90-0505, Jan. 1990.

[25]Goebel, S. G., "An Experimental Investigation of Compressible, Turbulent Mixing Layers," Ph.D. Thesis, Dept. of Mechanical and Industrial Engineering, Univ. of Illinois at Urbana-Champaign, Urbana, IL, May 1990.

[26]Chien, K.-Y., Ferguson, R. E., Kuhl, A. L., Glaz, H. M., and Colella, P., "Inviscid Dynamics of Two-Dimensional Shear Layers," AIAA Paper 91-1678, June 1991.

[27]Burr, R. F., and Dutton, J. C., "Numerical Simulations of Compressible and Reacting Temporal Mixing Layers and Implications for Modeling," AIAA Paper 91-1718, June 1991.

[28]Sigalla, L., Eberhardt, S., Greenough, J. A., Riley, J. J., and Soetrisno, M., "Numerical Simulation of Confined, Spatially-Developing Mixing Layers: Comparison to the Temporal Shear Layer," AIAA Paper 90-1462, July 1990.

[29]Leep, L. J., "Three-Dimensional Simulations of Compressible Mixing Layers: Visualizations and Statistical Analysis," M.S. Thesis, Dept. of Mechanical and Industrial Engineering, Univ. of Illinois at Urbana-Champaign, Urbana, IL, May 1992.

[30]McMurtry, P. A., Riley, J. J., and Metcalfe, R. W., "Effects of Heat Release on the Large-Scale Structure in Turbulent Mixing Layers," *Journal of Fluid Mechanics*, Vol. 199, Feb. 1989, pp. 297–332.

[31]Brown, G. L., and Roshko, A., "On Density Effects and Large Structures in Turbulent Mixing Layers," *Journal of Fluid Mechanics*, Vol. 64, June–July 1974, pp. 775–816.

[32]Bernal, L. P., and Roshko, A., "Streamwise Vortex Structures in Plane Mixing Layers," *Journal of Fluid Mechanics*, Vol. 170, Sept. 1986, pp. 499–525.